# SparseNeRF: Distilling Depth Ranking for Few-shot Novel View Synthesis

Guangcong Wang Zhaoxi Chen Chen Change Loy Ziwei Liu✉
S-Lab, Nanyang Technological University
{guangcong.wang,zhaoxi00,ccloy,ziwei.liu}@ntu.edu.sg

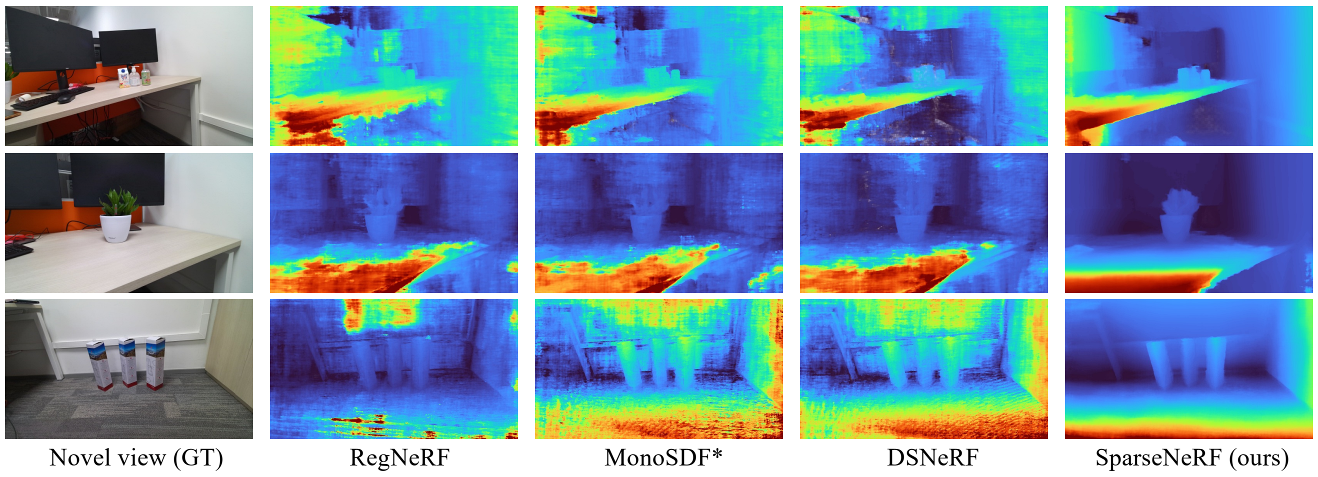

Figure 1: Comparing the state-of-the-arts RegNeRF [29], MonoSDF* [49], DSNeRF [11], and our SparseNeRF with three views for training (* denotes a re-implementation for our task). RegNeRF regularizes geometry with sparsity and continuity constraints. MonoSDF, and DSNeRF use scale-invariant depth constraints supervised by coarse depth maps. Our SparseNeRF uses robust depth ranking of coarse depth maps. SparseNeRF can synthesize realistic novel views and coherent geometric depth (Please refer to the supplementary material for rendered videos).

## Abstract

*Neural Radiance Field (NeRF) significantly degrades when only a limited number of views are available. To complement the lack of 3D information, depth-based models, such as DSNeRF and MonoSDF, explicitly assume the availability of accurate depth maps of multiple views. They linearly scale the accurate depth maps as supervision to guide the predicted depth of few-shot NeRFs. However, accurate depth maps are difficult and expensive to capture due to wide-range depth distances in the wild.*

*In this work, we present a new Sparse-view NeRF (**SparseNeRF**) framework that exploits depth priors from real-world inaccurate observations. The inaccurate depth observations are either from pre-trained depth models or coarse depth maps of consumer-level depth sensors. Since coarse depth maps are not strictly scaled to the ground-truth depth maps, we propose a simple yet effective constraint, a local depth ranking method, on NeRFs such that the expected depth ranking of the NeRF is consistent with that of the coarse depth maps in local patches. To preserve the spatial continuity of the estimated depth of NeRF, we further propose a spatial continuity constraint to encourage the consistency of the expected depth continuity of NeRF with coarse depth maps. Surprisingly, with simple depth ranking constraints, SparseNeRF outperforms all state-of-the-art few-shot NeRF methods (including depth-based models) on standard LLFF and DTU datasets. Moreover, we collect a new dataset NVS-RGBD that contains real-world depth maps from Azure Kinect, ZED 2, and iPhone 13 Pro. Extensive experiments on NVS-RGBD dataset also validate the superiority and generalizability of SparseNeRF. Project page is available at https://sparsenerf.github.io/.*

## 1. Introduction

Neural radiance fields (NeRFs) [27, 23, 1, 2, 35] have made tremendous progress in generating photo-realistic novel views of scenes by optimizing implicit function representations given a set of 2D input views. However, in a wide range of real-world scenarios, collecting dense views of a scene is often expensive and time-consuming [39]. Therefore, it is necessary to develop few-shot NeRFs that can be learned from sparse views without significant degradation.

Learning a NeRF from sparse views is a challenging problem due to under-constrained reconstruction conditions, especially in textureless areas. Directly applying NeRFs to few-shot scenarios suffers from dramatic degradation [29]. Recently, some methods have greatly improved the performance of few-shot NeRF, which can be categorized into three groups. **1)** The first group [29, 19, 17] is based on geometry constraints (sparsity and continuity regularizations) and high-level semantics. RegNeRF [29] regularized the geometry and appearance of patches rendered from unobserved viewpoints, and annealed the ray sampling space. InfoNeRF [19] imposed an entropy constraint of the density in each ray and a spatial smoothness constraint into the estimated images. However, since a scene often contains multiple layouts (**Figure 1**), sparsity and continuity geometric constraints of a few views cannot guarantee the complete 3D geometric reconstruction. **2)** The second group [48, 5] resorts to pre-training on similar scenes. For example, PixelNeRF [48] proposed to condition a NeRF on convolutional feature maps to learn high-level semantics from other scenes. **3)** The third group [11, 49] exploits depth maps and makes a linearity assumption of depth maps to supervise few-shot NeRFs. For example, DSNeRF [11] exploited sparse 3D points generated by COLMAP [33] or accurate depth maps [8] obtained by high-accuracy depth scanners and the Multi-View Stereo (MVS) algorithm. The depth maps are linearly scaled as supervision to guide the predicted depth of few-shot NeRFs. To use coarse depth maps, MonoSDF [49] uses a local patch-based scale-invariant depth constraint supervised by coarse depth maps instead of global depth maps. However, the scale-invariant depth constraint is strong for real-world depth maps from pre-trained depth models or consumer-level depth sensors.

Along the third group, we wish to explore more robust 3D priors from coarse depth maps to complement the under-constrained few-shot NeRF. To address this problem, we present SparseNeRF, a simple yet effective method that distills depth priors from pre-trained depth models [31] or inaccurate depth maps from consumer-level depth sensors (**Figure 3**), which can be easily obtained from real-world scenes. Deriving useful depth cues from such pre-trained models is non-trivial. In particular, although single-view depth estimation methods have achieved good visual performance, thanks to large-scale monocular depth datasets and large ViT models, they cannot yield accurate 3D depth information due to coarse depth annotations, dataset bias, and ill-posed 2D single-view images. The inaccurate depth information contradicts the density prediction of a NeRF when reconstructing each pixel of a 3D scene based on volume rendering. Directly scaling the coarse depth maps to a NeRF [11, 49] leads to inconsistent geometry against the expected depth of the NeRF.

Instead of directly supervising a NeRF with coarse depth priors, we relax hard depth constraints [11, 49] and distill robust local depth ranking from the coarse depth maps to a NeRF such that the depth ranking of a NeRF is consistent with that of coarse depth. That is, we supervise a NeRF with relative depth instead of absolute depth [11, 49]. To guarantee the spatial continuity of geometry, we further propose a spatial continuity constraint on depth maps such that the NeRF model imitates the spatial continuity of coarse depth maps. The accurate sparse geometry constraints from a limited number of views, combined with relaxed constraints including depth ranking regularization and continuity regularization, finally achieve promising novel view synthesis (**Figure 1**). It is noteworthy that SparseNeRF does not increase the running time during inference as it only exploits depth priors from pre-trained depth models or consumer-level sensors during the training stage (**Figure 2**). In addition, SparseNeRF is a plug-and-play module that can be easily integrated into various NeRFs.

The main contribution of this paper is **1)** SparseNeRF, a simple yet effective method that distills local depth ranking priors from pre-trained depth models. With the help of the local depth ranking constraint, SparseNeRF significantly improves the performance of few-shot novel view synthesis over the state-of-the-art models (including depth-based NeRF methods). To preserve the coherent geometry of a scene, we propose a spatial continuity distillation constraint that encourages the spatial continuity of NeRF to be similar to that of the pre-trained depth model. Both depth ranking prior and spatial continuity distillation are new in the literature on NeRF. **2)** Apart from SparseNeRF, we also contribute a new dataset, NVS-RGBD, which contains coarse depth maps from Azure Kinect, ZED 2, and iPhone 13 Pro. **3)** Extensive experiments on the LLFF, DTU, and NVS-RGBD datasets demonstrate that SparseNeRF achieves a new state-of-the-art performance in few-shot novel view synthesis.

## 2. Related Work

**Neural Radiance Fields.** NeRF [27] has made great success in synthesizing novel views of complex scenes. Block-NeRF [39], CityNeRF [45], and Mega-NeRF [40] scaled the standard NeRF up to city-scale or urban-scale scenes. NeRF−− [42], GNeRF [24], and BARF [21] relaxed the requirements of NeRFs and synthesized novel views without perfect camera poses. Some works attempted to improve NeRFs by considering anti-aliasing [1], sparse 3D grids with spherical harmonics [13]. Some methods [30, 20, 44, 14] extended NeRFs to dynamic scenes. To achieve real-time novel view synthesis, a wide range of approaches [47, 38, 22, 43, 15, 32, 16, 28] attempted to speed up the standard NeRF. These methods do not focus on generating novel views with a few views. In this paper, we study using sparse views to train a NeRF for novel view synthesis.

**Few-shot Novel View Synthesis.** There are increasing studies on few-shot novel view synthesis. The existing few-shot NeRF methods can be categorized into three groups. **First**, some methods exploit continuity constraints on geometry or object semantics. For example, RegNeRF [29] imposed a continuity constraint on geometry and regularized the appearance of patches from unobserved viewpoints with a flow model. InfoNeRF [19] proposed a ray entropy minimization regularization to encourage the density to be as sparse as possible along a ray, and used a ray information gain reduction regularization to constrain the continuous depth of neighbor rays. **Second**, some methods attempt to pe-train a NeRF on other similar scenes and fine-tune the NeRF on the target scene. For example, PixelNeRF [48] conditioned a NeRF on image inputs in a fully convolutional manner, allowing the model to learn scene priors from other scenes and reduce the requirement of dense views. MVSNeRF [5] leveraged plane-swept cost volumes for geometry-aware scene reasoning, and combined it with physically based volume rendering. Similar to PixelNeRF, MVSNeRF was first trained on other real scenes and was finetuned on target scenes to evaluate its effectiveness and generalizability. **Third**, depth-based models [11, 49] use available depth information to supervise the training of NeRFs. DSNeRF [11] exploited sparse 3D points generated by COLMAP [33] or accurate depth maps [8] obtained by high-accuracy depth scanners. Different from these depth-based models, SparseNeRF distills robust depth ranking from pre-trained depth models or coarse depth maps from consumer-level sensors. Some single-view synthesis methods [46, 4] either allow new generative objects from unseen views or focus on specific objects, e.g., face. Our method mainly focuses on the reconstruction of general scenes.

## 3. Our Approach

We present SparseNeRF to synthesize novel views given sparse view inputs. Single-view depth estimation is a long-standing computer vision task, aiming to predict a depth map given a single image. In this paper, we are interested in mining the depth priors encapsulated in pre-trained models of single-view depth estimation or coarse depth maps captured by consumer-level depth sensors. However, due to coarse annotations of single-view depth maps, (*e.g.*, user clicks [6], RGB-D [34, 37], and laser/stereo [25]), dataset bias, and imperfect depth estimation models, it is challenging to obtain accurate 3D depth estimation given 2D single-view images. As for consumer-level depth sensors, it still struggles to capture accurate depth maps (**Figure 3**). Driven by these observations, our goal is to make use of the coarse depth maps and distill useful depth priors to guide the learning of a NeRF.

### 3.1. Preliminary and Problem Formulation

**Neural Radiance Fields.** Let a NeRF [27] be a mapping function $f$ that maps a 3D spatial location $\mathbf{x}$ and a viewing direction $\mathbf{d}$ into a volume density $\sigma$ and a color value $\mathbf{c}$. The $f$ is a neural network consisting of eight perceptron (MLP) layers parameterized by $\theta$, which is given by $f_\theta : (\gamma(\mathbf{x}), \gamma(\mathbf{d})) \mapsto (\sigma, \mathbf{c})$, where $\gamma$ is a positional encoding. For each expected pixel color $\hat{C}(\mathbf{r})$, it is rendered by casting a ray $\mathbf{r}(t) = \mathbf{o} + t\mathbf{d}$ with near and far bounds $t_n$ and $t_f$. We evenly partition $[t_n, t_f]$ into $N$ points $(t_1, t_2, ..., t_N)$ along a ray $\mathbf{r}$ and compute expected pixel color $\hat{C}(\mathbf{r})$ by $\hat{C}(\mathbf{r}) = \sum_{i=1}^{N} \mathbf{c}_i^*$. The weighted color $\mathbf{c}_i^*$ of a 3D point is computed by $\mathbf{c}_i^* = w_i \mathbf{c}_i$, where $w_i = T_i(1 - \exp(-\sigma_i\delta_i))$, $T_i = \exp(-\sum_{j=1}^{i-1} \sigma_j\delta_j)$ and $\delta_i = t_i - t_{i-1}$. The NeRF reconstruction loss is given by

$$\mathcal{L}_{\text{nerf}} = \sum_{\mathbf{r}\in R} ||\hat{C}(\mathbf{r}) - C(\mathbf{r})||^2, \qquad (1)$$

where $\hat{C}(\mathbf{r})$ are rendered color blended by $N$ samples. $C(\mathbf{r})$ is the ground-truth pixel color. We use coarse-to-fine sampling as discussed in the vanilla NeRF [27]. Here we omit the fine rendering for simplification.

**Problem Formulation.** Vanilla NeRFs aim to learn a mapping function $f_\theta$ with $K_d$ dense views by optimizing a color reconstruction loss in **Eq. (1)**. In this work, we aim to study few-shot NeRF when only $K_s$ sparse views are available ($K_s \ll K_d$). Let $H$ and $W$ denote the height and width of an image, we have $HWK_s$ rays as color reconstruction constraints. Without considering view directions $\mathbf{d}$ and image continuity assumptions (i.e., $\mathbf{c}_i^*$ is independent of $\mathbf{c}_j^*$ when $i \neq j$), suppose we have a $N_c \times N_c \times N_c$ discrete cubic volume to be optimized, which contains $N_c^3$ weighted color variables $\mathbf{c}_i^*$. We have $N_c^3$ variables $\mathbf{c}_i^*$ and $HWK_s$ constraints. Ideally, we are able to solve a discrete cube of edge length $N_c = \sqrt[3]{HWK_s}$. That is, we can sample $\sqrt[3]{HWK_s}$ for each edge of a cubic volume. Take $H = W = 512$ and $K_s = 3$ as an example, we have $N_c \approx 92$, which is far from reconstructing a continuous radiance field. To address this under-constrained optimization problem of few-shot NeRF, an intuitive way is to introduce reasonable regularization terms to constrain few-shot NeRFs conditioned on input $\mathbf{x}$, $\mathbf{d}$, and $C(\mathbf{r})$. A general formulation is given by

$$\mathcal{L} = \mathcal{L}_{\text{nerf}} + \lambda\mathcal{R}(\mathbf{x}, \mathbf{d}, C(\mathbf{r})), \qquad (2)$$

where $\mathcal{R}$ is a regularization term.

**Remark.** RegNeRF [29] and InfoNeRF [19] tackles this problem by introducing regularization terms on continuous depth constraint from unobserved viewpoints, sparsity

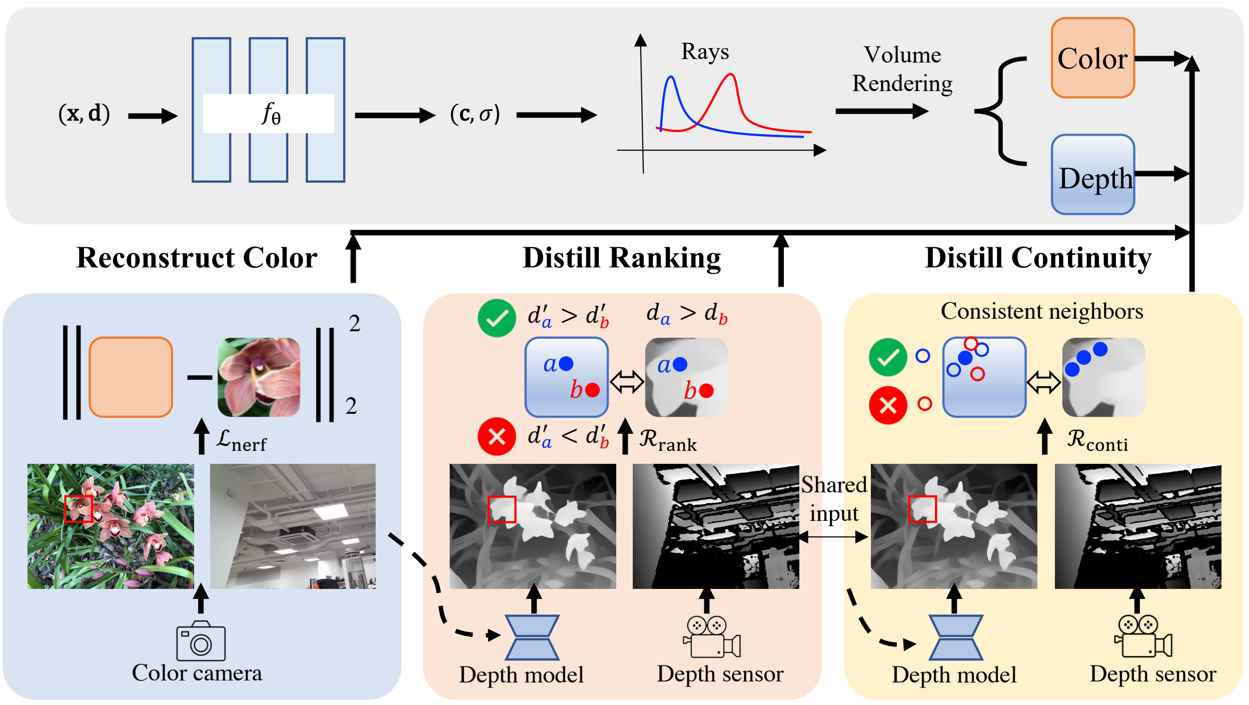

Figure 2: Framework Overview. SparseNeRF consists of two streams, i.e., NeRF and depth prior distillation. As for NeRF, we use Mip-NeRF as the backbone. we use a NeRF reconstruction loss $\mathcal{L}_{\text{nerf}}$. As for depth prior distillation, we distill depth priors from a pre-trained depth model. Specifically, we propose a local depth ranking regularization and a spatial continuity regularization to distill robust depth priors from coarse depth maps.

of density on rays, and patch-based semantic constraint on color appearance. Depth-based models, such as DSNeRF [11] and MonoSDF [49], directly regress depth by leveraging sparse 3D points or deriving ground-truth depth maps with accurate absolute depth maps. Different from them, we propose to use a robust relative depth regularization from coarse depth maps of pre-trained depth models or consumer-level depth sensors.

## 3.2. Overview of SparseNeRF

The pipeline of SparseNeRF is illustrated in **Figure 2**. SparseNeRF mainly consists of four components, i.e., a neural radiance field (NeRF), a color reconstruction module, a depth ranking distillation module, and a spatial continuity distillation module. Specifically, we use Mip-NeRF [1] as the backbone and apply an MSE loss for color reconstruction $\mathcal{L}_{\text{nerf}}$. As for depth prior distillation, we either use a pre-trained depth model to estimate depth maps or capture coarse depth maps with consumer-level depth sensors. We use a vision transformer (DPT) [31] that is trained on a large-scale mixed depth dataset (1.4M images with various depth annotations) that covers a wide range of scenes. Therefore, DPT is able to provide general depth priors. Since single-view depth estimation is coarse, we carefully design a local depth ranking regularization and a spatial continuity regularization, which distills robust depth priors from coarse maps to the NeRF.

## 3.3. Local Depth Ranking Distillation

Single-view depth estimation is a challenging computer vision task, which aims at predicting a depth map of a scene given a single image as input. Due to dataset bias, coarse depth annotations, and imperfect neural models, it is difficult to achieve accurate depth prediction. Depth maps captured by consumer-level sensors are also inaccurate due to wide-range depth distances. Directly using coarse depth maps to supervise a NeRF leads to ambiguous rendered novel view synthesis. To avoid the error of coarse depth maps, we relax the depth constraint and exploit the robust depth ranking prior. Given a pair of pixels in a single image, the depth ranking regularization only considers which point is nearer or farther. However, when the scene is complex, even depth ranking is not accurate. As shown in **Figure 4**, it is easy for depth estimation models to compare the depth ranking of green and cyan points, but it is hard to estimate the depth ranking of green and red points. It implies that the depth ranking becomes unreliable with the spatial distance increases.

Motivated by these observations, we propose a local depth ranking distillation method that distills depth ranking priors from coarse depth maps to a NeRF. On one hand, given a local patch $P$ of an RGB image $I$ with a pose $p$. We compute the depth $d_{\mathbf{r}}$ of the rays that trace from $P$ by $d_{\mathbf{r}} = \sum_{i=1}^{N} w_i t_i$. On the other hand, we use pre-trained depth DPT [31] to estimate the depth of $I$ and crop a local

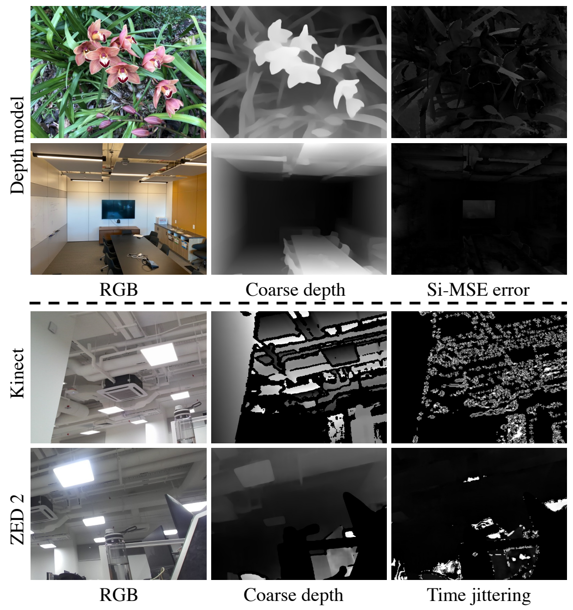

Figure 3: Two types of coarse depth maps. Top: predicted by a pre-trained depth model. Bottom: captured by Azure Kinect and ZED 2 depth sensors. Si-MSE is a scale-invariant depth error derived by minimizing $||w\hat{d}+b-d||$, where $\hat{d}$ and $d$ denote coarse depth maps and pseudo-ground-truth predicted by dense-view NeRF. Time jittering refers to the difference between two depth maps captured by a static camera within a small time interval.

patch $d_{\text{dpt}}$ with the same spatial location as $d_{\mathbf{r}}$. We perform the depth ranking distillation by transferring the depth ranking knowledge from $d_{\text{dpt}}$ to $d_{\mathbf{r}}$. Let $k1$ and $k2$ be the indices of 2D spatial coordinate of $d_{\text{dpt}}$ and $d_{\mathbf{r}}$. The depth ranking regularization is given by

$$\mathcal{R}_{\text{rank}} = \sum_{d_{\text{dpt}}^{k1} \leq d_{\text{dpt}}^{k2}} \max(d_{\mathbf{r}}^{k1} - d_{\mathbf{r}}^{k2} + m, 0), \qquad (3)$$

where $m$ is a small margin that allows depth ranking errors. In **Eq.** (3), we randomly sample two depth pixels of $d_{\text{dpt}}$, as denoted as $d_{\text{dpt}}^{k1}$ and $d_{\text{dpt}}^{k2}$, $d_{\text{dpt}}^{k1} \leq d_{\text{dpt}}^{k2}$. If the depth rankings of $d_{\text{dpt}}$ and $d_{\mathbf{r}}$ are not consistent, i.e., $d_{\mathbf{r}}^{k1} > d_{\mathbf{r}}^{k2}$ and $d_{\text{dpt}}^{k1} \leq d_{\text{dpt}}^{k2}$, we punish the NeRF. We encourage the corresponding depth estimated by NeRF to satisfy the consistent depth ranking of the pre-trained model. We clip the large depth value and normalize the depth map for depth sensors. For depth models, we use relative inverse depth.

### 3.4. Spatial Continuity Distillation

The local depth ranking constraint guarantees that the predicted depth map estimated by NeRF is consistent with the DPT's depth map. However, it does not constrain the spatial continuity of the depth map. We distill spatial continuity priors from the depth model DPT, which allows large displacement across several depth pixels. If neighbor depth pixels are continuous on the depth map of DPT, we constrain the corresponding depth pixels of NeRF to be continuous. The spatial continuity regularization is given by

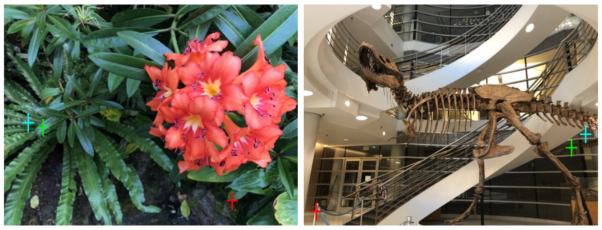
Figure 4: Motivation of local depth ranking. It is easy for depth estimation models to tell the green point is nearer than the cyan point, but it is hard to compare green and red points. Best viewed by zooming in.

$$\mathcal{R}_{\text{conti}} = \sum_{k1} \sum_{d_{\text{dpt}}^{k2} \in \text{KNN}(d_{\text{dpt}}^{k1})} \max(|d_{\mathbf{r}}^{k1} - d_{\mathbf{r}}^{k2}| - m', 0), \qquad (4)$$

where $\text{KNN}(\cdot)$ returns k-nearest neighbors measured by depth values within a small region, *e.g.*, $6 \times 6$ patch. $m'$ is a small margin that allows small depth differences between neighbor pixels.

**Full Objective Loss.** The full objective loss of SparseNeRF is formulated by

$$\mathcal{L} = \mathcal{L}_{\text{nerf}} + \lambda \mathcal{R}_{\text{rank}} + \gamma \mathcal{R}_{\text{conti}}, \qquad (5)$$

where $\lambda$ and $\gamma$ control the importance of the regularization terms. In practice, we set $\lambda = 0.2$, $\gamma = 0.02$, $m = m' = 1.0 \times 10^{-4}$.

## 4. NVS-RGBD Dataset

The popular benchmark LLFF [26] on NeRFs is featured with 1) forward-facing and 2) object-centric. Moreover, we focus on 3) consumer-level depth sensors instead of expensive scanners [9]. We 4) study stand-alone depth cameras instead of complex calibrated structured multiple camera system [10], and 5) collect from real-world scenes instead of synthesized 3D assets [36]. Few RGBD datasets satisfy all of the requirements. Therefore, we collect a new dataset NVS-RGBD that contains real-world depth maps captured by consumer-level depth sensors, including Azure Kinect, ZED 2, and iPhone 13 Pro. We collect 8 scenes for each sensor and obtain 24 scenes. The depth maps of Azure Kinect often contain noises around object edges. The depth maps of ZED 2 look smooth but unstable and incorrect when observing time jittering (**Figure** 3). The poses are computed via COLMAP. We collect indoor scenes for ZED 2 and Kinect. For iPhone, we collect both indoor and outdoor scenes. All the scenes are object-centric. Depth maps obtained from sensors have different artifacts coming from the sensor noises. Depth maps obtained from pre-trained models are not linear-invariant to the ground truth. Please refer to the supplementary material for the details.

## 5. Experiments

**Datasets.** We conduct experiments on the LLFF [26], DTU [18], and NVS-RGBD datasets. LLFF contains 8 complex forward-facing scenes. Following RegNeRF [29], we use every 8-th image as the held-out test set, and evenly sample sparse views from the remaining images for training. Different from LLFF, DTU is an object-level dataset. Following PixNeRF [48, 29], we use the same 15 scenes in our experiments. On the DTU dataset, the background of these scenes is a white table or a black background, which has few textures. As mentioned in RegNeRF, we mask the background during inference to avoid background bias. We use the same evaluation protocol for a fair comparison. On the NVS-RGBD dataset, for each scene, we use 3 views for training and the rest views for inference. For LLFF and DTU, we use pre-trained depth maps to implement our method. For NVS-RGBD, we use coarse depth maps captured by depth sensors.

**Evaluation Metrics.** We adopt four evaluation metrics in the experiments, i.e., PSNR, SSIM [41], LPIPS [50], and depth error [11]. Depth error is a scale-invariant MSE derived by minimizing $||w\hat{d} + b - d||$, where $\hat{d}$ and $d$ denote coarse depth maps and pseudo-ground-truth depth maps predicted by dense-view NeRF. Note that we only use dense views to train a good NeRF to generate pseudo-ground-truth depth maps for evaluation.

**Implementation Details.** We implement SparseNeRF based on the JAX [3]. We use the Adam optimizer for the learning of SparseNeRF. We use an exponential learning rate, which decays from $2 \times 10^{-3}$ to $2 \times 10^{-5}$. The batch size is set to 4096. For each scene, we use one GPU-v100 for both training and inference. We use the same backbone and sampled points compared with prior arts. It takes about 1.5 hours for training a scene with 1 GPU V100.

### 5.1. Comparisons on LLFF

We compare SparseNeRF with state-of-the-art methods on the LLFF dataset, including SRF [7], PixelNeRF [48], MVSNeRF [5], Mip-NeRF [1], DietNeRF [17], RegNeRF [29], and DSNeRF [11]. Among them, SRF, PixelNeRF, and MVSNeRF are pre-trained on other similar scenes to exploit high-level semantics. Mip-NeRF is the state-of-the-art NeRF designed for dense-view training. InfoNeRF and RegNeRF mainly constrain sparsity and continuity of geometry or natural appearance semantics. More precisely, the compared methods can be classified into four groups. In the first group, SRF, PixelNeRF, and MVSNeRF are pre-trained in the large-scale DTU datasets (88 scenes) and are directly tested on the LLFF dataset. In the second group, SRF, PixelNeRF, and MVSNeRF are pre-trained on DTU and fine-tuned on LLFF per scene. The third group includes Mip-NeRF, DietNeRF, and RegNeRF. They uses geometry continuity and semantic constraints. The fourth group distills knowledge from depth maps. The compared results are shown in **Table 1**. We can see that the proposed SparseNeRF achieves the best performance in PSNR, SSIM, and LPIPS. Note that the first and second groups have to pre-train on lots of other scenes. SparseNeRF achieves better results than DSNeRF because the depth ranking is more robust than the absolute scale-invariant constraint.

Table 1: Quantitative Comparison on LLFF with three views. There are four groups. The first group denotes models that are pre-trained on other scenes and tested on a target scene (P). The second group requires further finetuning on a target scene (P&FT). The third group uses geometry and semantic constraints (geo. & sem.). The fourth group distills depth knowledge (depth KD).

| | Setting | PSNR ↑ | SSIM ↑ | LPIPS ↓ |
|---|---|---|---|---|
| SRF [7] | P | 12.34 | 0.250 | 0.591 |
| PixelNeRF [48] | | 7.93 | 0.272 | 0.682 |
| MVSNeRF [5] | | 17.25 | 0.557 | 0.356 |
| SRF ft [7] | P&FT | 17.07 | 0.436 | 0.529 |
| PixelNeRF ft [48] | | 16.17 | 0.438 | 0.512 |
| MVSNeRF ft [5] | | 17.88 | 0.584 | 0.327 |
| Mip-NeRF [1] | geo. & sem. | 14.62 | 0.351 | 0.495 |
| DietNeRF [17] | | 14.94 | 0.370 | 0.496 |
| RegNeRF [29] | | 19.08 | 0.668 | 0.283 |
| DSNeRF [11] | depth KD | 18.45 | 0.632 | 0.388 |
| **SparseNeRF (Ours)** | | **19.86** | **0.714** | **0.243** |

We provide qualitative analysis on LLFF, as shown in **Figure 5**. It is observed that PixelNeRF and MVSNeRF tend to generate ambiguous pixels. The reason is that they integrate CNN features into NeRFs. CNN features can provide high-level semantics to infer under-constrained textures but suffer pixel-level inference. MipNeRF is designed for dense-view synthesis without considering the under-constrained problem, leading to degraded geometry artifacts. Compared with RegNeRF, SparseNeRF uses robust depth priors from pre-trained depth models, which can handle challenging scene geometry with better performance.

### 5.2. Comparisons on DTU

Similar to the LLFF dataset, we conduct four-group comparisons on the DTU dataset, as shown in **Table 2**. In this first group, given a target scene, SRF, PixelNeRF, and MVSNeRF are pre-trained on other DTU scenes and are tested on the target scene. In the second group, these three methods are further fine-tuned on the target scene. In the third group, we compare Mip-NeRF, DietNeRF, and RegNeRF. Note that for the pre-trained models, they split DTU as a training set (88 scenes) and a test set (15 scenes). Since the training set and the test set contains similar scenes, a test scene shares a similar distribution (e.g., similar backgrounds) with training scenes. Pre-training on other scenes greatly benefits a target scene. Therefore, SRF, PixelNeRF, and MVSNeRF also greatly achieve promising results. Finally, we compare depth-based DSNeRF [11], which dis-

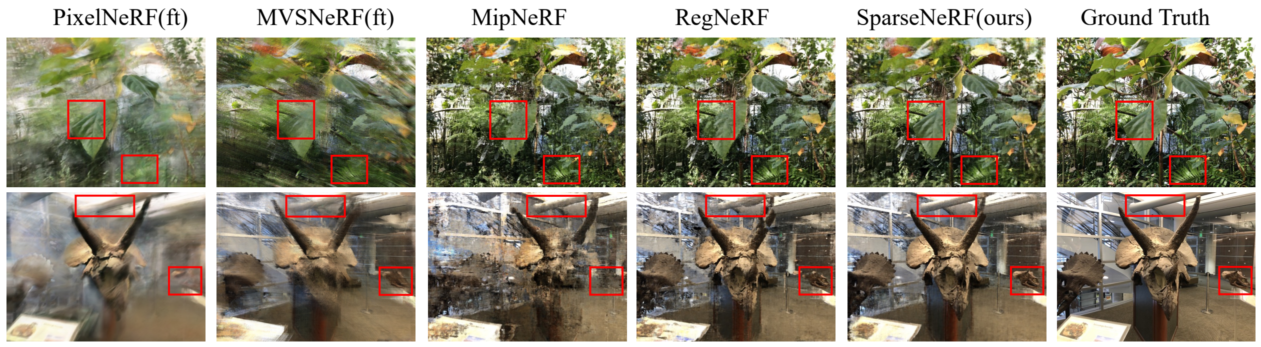

Figure 5: Visual comparisons on the LLFF dataset with three views. Red boxes denote compared regions. SparseNeRF achieves consistent improvement in different scenes.

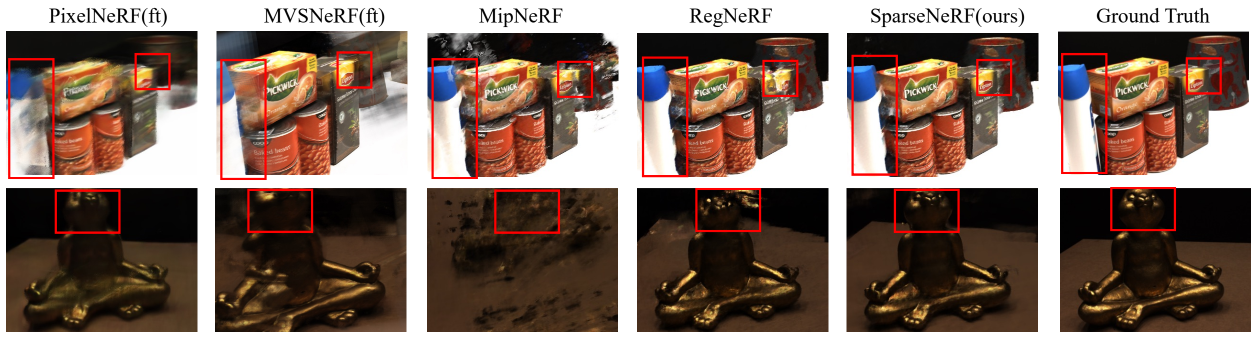

Figure 6: Visual comparisons on the DTU dataset with three views. Red boxes denote compared regions. SparseNeRF achieves consistent improvement in different scenes.

Table 2: Quantitative Comparison on DTU with three views. The first group is pre-trained on other scenes and tested on a target scene (P). The second group requires further finetuning on a target scene (P&FT). The third group uses geometry and semantic constraints (geo. & sem.). The fourth group distills depth knowledge (depth KD).

| | **Setting** | **PSNR ↑** | **SSIM ↑** | **LPIPS ↓** |
|---|---|---|---|---|
| SRF [7] | P | 15.32 | 0.671 | 0.304 |
| PixelNeRF [48] | | 16.82 | 0.695 | 0.270 |
| MVSNeRF [5] | | 18.63 | 0.769 | 0.197 |
| SRF ft [7] | P&FT | 15.68 | 0.698 | 0.281 |
| PixelNeRF ft [48] | | 18.95 | 0.710 | 0.269 |
| MVSNeRF ft [5] | | 18.54 | 0.769 | 0.197 |
| Mip-NeRF [1] | geo. & sema. | 8.68 | 0.571 | 0.353 |
| DietNeRF [17] | | 11.85 | 0.633 | 0.314 |
| RegNeRF [29] | | 18.89 | 0.745 | 0.190 |
| DSNeRF [11] | depth KD | 16.90 | 0.570 | 0.450 |
| **SparseNeRF(Ours)** | | **19.47** | **0.829** | **0.183** |

tills the scale-invariant depth constraint for supervision. Compared with these methods, SparseNeRF still achieves the best performance without pre-training on other scenes, yielding 19.47, 0.829, and 0.183 on the PSNR, SSIM, LPLPS metrics, respectively. We provide a qualitative analysis, as shown in **Figure 6**. SparseNeRF achieves better visual results over previous state-of-the-art methods.

## 5.3. Comparisons on NVS-RGBD

We then implement three state-of-the-art methods on our new NVS-RGBD dataset, including RegNeRF [29], DSNeRF [11], and MonoSDF [49]. All of them are optimized per scene without pre-training on the other scenes. RegNeRF adopted continuous geometry assumptions from unobserved viewpoints. DSNeRF uses a global scale-invariant depth constraint to supervise NeRFs. MonoSDF mainly focuses on implicit surface reconstruction. It is assumed that local patches of depth maps from monocular cameras satisfy $d^{'} = wd + b$ where $d$ is predicted by the pre-trained model and $d^{'}$ is then computed by the NeRF. In **Table 3**, we observe that SparseNeRF achieves better performance compared with these prior arts. We provide a qualitative analysis in **Figure 7**, demonstrating the superiority of SparseNeRF over previous state-of-the-art methods.

Table 3: Comparison with State of the Arts on NVS-RGBD. * denotes a new implementation from related tasks.

| | Metrics | PSNR↑ | SSIM↑ | LPIPS↓ | depth err↓ |
|---|---|---|---|---|---|
| Kinect | RegNeRF [29] | 25.78 | 0.902 | 0.158 | $5.9\times10^{-3}$ |
| | DSNeRF [11] | 25.91 | 0.901 | 0.157 | $4.8\times10^{-3}$ |
| | MonoSDF* [49] | 25.50 | 0.901 | 0.161 | $5.5\times10^{-3}$ |
| | **SparseNeRF(ours)** | **26.28** | **0.913** | **0.155** | $\mathbf{3.9\times10^{-3}}$ |
| ZED 2 | RegNeRF [29] | 24.98 | 0.875 | 0.206 | $3.5\times10^{-3}$ |
| | DSNeRF [11] | 24.97 | 0.877 | **0.198** | $3.1\times10^{-3}$ |
| | MonoSDF* [49] | 24.54 | 0.873 | 0.212 | $3.2\times10^{-3}$ |
| | **SparseNeRF(ours)** | **26.22** | **0.893** | **0.198** | $\mathbf{2.4\times10^{-3}}$ |

## 5.4. Ablation Studies and Further Analyses

**Effectiveness of Depth Distillation.** To validate the effectiveness of the depth distillation, we isolate the depth con-

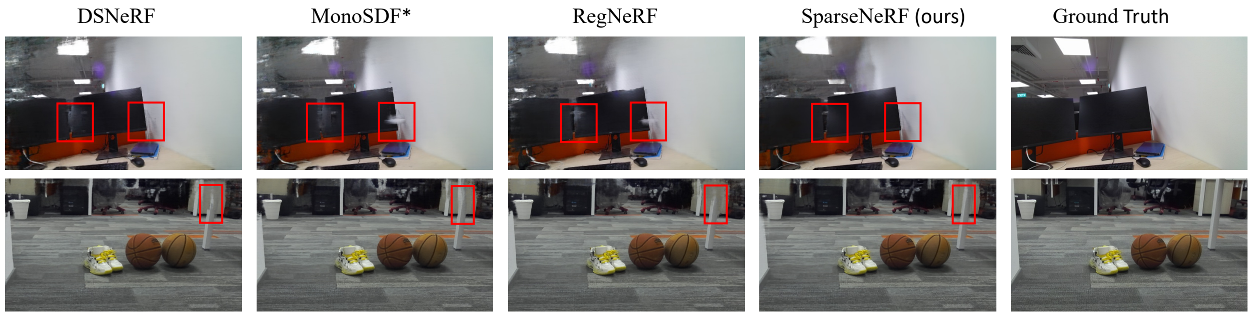

Figure 7: Visual comparisons on the NVS-RGBD dataset with three views. Red boxes denote compared regions. SparseNeRF achieves consistent improvement in different scenes.

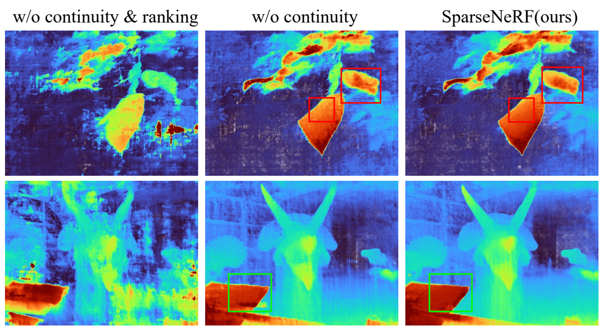

Figure 8: Ablation study on visual effect. The three columns denote "w/o continuity and ranking distillation", "w/o continuity distillation", and "w continuity and ranking distillation" (SparseNeRF, ours), respectively.

Table 4: Comparison of Depth Ranking and Depth scaling.

| LLFF | PSNR↑ | SSIM↑ | LPIPS↓ | depth err↓ |
|---|---|---|---|---|
| baseline | 19.08 | 0.668 | 0.283 | $10.1\times10^{-3}$ |
| w/ depth scaling | 18.45 | 0.632 | 0.388 | $8.9\times10^{-3}$ |
| **w/ depth ranking** | **19.86** | **0.714** | **0.243** | $\mathbf{6.3\times10^{-3}}$ |

straint and keep other modules unchanged. As shown in the first and third rows of **Table 4**, it is observed that without the local depth ranking distillation, SparseNeRF degrades 0.78, 0.046, 0.040, $5.8 \times 10^{-3}$ on PSNR, SSIM, LPIPS, and depth error, which demonstrates the effectiveness of the depth distillation. We further study the depth maps from unobserved views. The ablation study of visual effect is shown in **Figure 8**. It shows that depth ranking greatly improves performance in geometry. Spatial continuity regularization further improves the detailed coherence of scenes.

**Further Analyses on Depth Ranking and Depth Scaling.** To validate the robustness of local depth ranking, we compare depth ranking regularization and depth scaling regularization on LLFF, which is similar to **Section 5.3** and **Table 3**. We use the idea from MonoSDF [49], which mainly focuses on implicit surface reconstruction. Since the single-view depth estimation is not accurate, the linear depth scaling constraint is too strong such that depth distillation misleads the learning of the NeRF. **Figure 3** shows two cases of scale-invariant errors. Instead, depth ranking relaxes the constraint and only focuses on depth comparison, which is more robust than depth scaling. As shown in **Table 4**, depth ranking performs better than depth scaling on LLFF.

Table 5: Impact of different pre-trained depth models.

| LLFF | PSNR↑ | SSIM↑ | LPIPS↓ | depth err↓ |
|---|---|---|---|---|
| Baseline | 19.08 | 0.668 | 0.283 | $10.1\times10^{-3}$ |
| MiDaS small | 19.35 | 0.681 | 0.279 | $6.9\times10^{-3}$ |
| DPT Hybrid | 19.86 | 0.714 | 0.243 | $6.3\times10^{-3}$ |
| DPT Large | 19.86 | 0.706 | 0.251 | $6.4\times10^{-3}$ |

**Impact of Different Pre-trained Depth Models.** We test our method on three depth estimation models, i.e., MiDaS small, DPT Hybrid, and DPT Large. As shown in **Table 5**, all of the depth models are better than the baseline. DPT Hybrid and DPT Large achieve comparable results, which are better than MiDaS small. We use DPT Hybrid to estimate coarse depth maps on the LLFF and DTU datasets.

**More Applications.** SparseNeRF could have a wide range of applications due to its promising results. We provide two applications on iPhone 13 Pro. Please refer to the supplementary material for more experiments.

## 6. Conclusion

In this paper, we propose a SparseNeRF framework that synthesizes novel views with sparse view inputs. To tackle the under-constrained few-shot NeRF problem, we propose a local depth ranking regularization that distills the depth ranking prior from coarse depth maps. To preserve the spatial continuity of geometry, we propose a spatial continuity regularization that distills the depth continuity priors. With the proposed depth priors, SparseNeRF achieves a new state-of-the-art performance on three datasets.

**Limitation.** SparseNeRF significantly improves the performance of few-shot NeRF, but cannot be generalized to occluded views that are unobserved in the training views.

**Potential Negative Impact.** SparseNeRF focuses on scene synthesis. It might be misused to create misleading content.

## References

[1] Jonathan T Barron, Ben Mildenhall, Matthew Tancik, Peter Hedman, Ricardo Martin-Brualla, and Pratul P Srinivasan. Mip-nerf: A multiscale representation for anti-aliasing neural radiance fields. In *Proceedings of the IEEE/CVF International Conference on Computer Vision*, pages 5855–5864, 2021. 1, 2, 4, 6, 7

[2] Jonathan T Barron, Ben Mildenhall, Dor Verbin, Pratul P Srinivasan, and Peter Hedman. Mip-nerf 360: Unbounded anti-aliased neural radiance fields. In *Proceedings of the IEEE/CVF Conference on Computer Vision and Pattern Recognition*, pages 5470–5479, 2022. 1

[3] James Bradbury, Roy Frostig, Peter Hawkins, Matthew James Johnson, Chris Leary, Dougal Maclaurin, George Necula, Adam Paszke, Jake VanderPlas, Skye Wanderman-Milne, and Qiao Zhang. JAX: composable transformations of Python+NumPy programs, 2018. 6, 15

[4] Eric R Chan, Connor Z Lin, Matthew A Chan, Koki Nagano, Boxiao Pan, Shalini De Mello, Orazio Gallo, Leonidas J Guibas, Jonathan Tremblay, Sameh Khamis, et al. Efficient geometry-aware 3d generative adversarial networks. In *Proceedings of the IEEE/CVF Conference on Computer Vision and Pattern Recognition*, pages 16123–16133, 2022. 3

[5] Anpei Chen, Zexiang Xu, Fuqiang Zhao, Xiaoshuai Zhang, Fanbo Xiang, Jingyi Yu, and Hao Su. Mvsnerf: Fast generalizable radiance field reconstruction from multi-view stereo. In *Proceedings of the IEEE/CVF International Conference on Computer Vision*, pages 14124–14133, 2021. 2, 3, 6, 7

[6] Weifeng Chen, Zhao Fu, Dawei Yang, and Jia Deng. Single-image depth perception in the wild. *Advances in neural information processing systems*, 29, 2016. 3

[7] Julian Chibane, Aayush Bansal, Verica Lazova, and Gerard Pons-Moll. Stereo radiance fields (srf): Learning view synthesis for sparse views of novel scenes. In *Proceedings of the IEEE/CVF Conference on Computer Vision and Pattern Recognition*, pages 7911–7920, 2021. 6, 7

[8] Sungjoon Choi, Qian-Yi Zhou, Stephen Miller, and Vladlen Koltun. A large dataset of object scans. *arXiv preprint arXiv:1602.02481*, 2016. 2, 3

[9] Sungjoon Choi, Qian-Yi Zhou, Stephen Miller, and Vladlen Koltun. A large dataset of object scans. *arXiv:1602.02481*, 2016. 5

[10] Angela Dai, Angel X. Chang, Manolis Savva, Maciej Halber, Thomas Funkhouser, and Matthias Nießner. Scannet: Richly-annotated 3d reconstructions of indoor scenes. In *Proc. Computer Vision and Pattern Recognition (CVPR), IEEE*, 2017. 5

[11] Kangle Deng, Andrew Liu, Jun-Yan Zhu, and Deva Ramanan. Depth-supervised nerf: Fewer views and faster training for free. In *Proceedings of the IEEE/CVF Conference on Computer Vision and Pattern Recognition*, pages 12882–12891, 2022. 1, 2, 3, 4, 6, 7, 12

[12] Zhiwen Fan, Yifan Jiang, Peihao Wang, Xinyu Gong, Dejia Xu, and Zhangyang Wang. Unified implicit neural stylization. In *European Conference on Computer Vision*, pages 636–654. Springer, 2022. 12

[13] Sara Fridovich-Keil, Alex Yu, Matthew Tancik, Qinhong Chen, Benjamin Recht, and Angjoo Kanazawa. Plenoxels: Radiance fields without neural networks. In *Proceedings of the IEEE/CVF Conference on Computer Vision and Pattern Recognition (CVPR)*, pages 5501–5510, June 2022. 2

[14] Guy Gafni, Justus Thies, Michael Zollhofer, and Matthias Nießner. Dynamic neural radiance fields for monocular 4d facial avatar reconstruction. In *Proceedings of the IEEE/CVF Conference on Computer Vision and Pattern Recognition*, pages 8649–8658, 2021. 2

[15] Stephan J Garbin, Marek Kowalski, Matthew Johnson, Jamie Shotton, and Julien Valentin. Fastnerf: High-fidelity neural rendering at 200fps. In *Proceedings of the IEEE/CVF International Conference on Computer Vision*, pages 14346–14355, 2021. 3

[16] Peter Hedman, Pratul P Srinivasan, Ben Mildenhall, Jonathan T Barron, and Paul Debevec. Baking neural radiance fields for real-time view synthesis. In *Proceedings of the IEEE/CVF International Conference on Computer Vision*, pages 5875–5884, 2021. 3

[17] Ajay Jain, Matthew Tancik, and Pieter Abbeel. Putting nerf on a diet: Semantically consistent few-shot view synthesis. In *Proceedings of the IEEE/CVF International Conference on Computer Vision*, pages 5885–5894, 2021. 2, 6, 7

[18] Rasmus Jensen, Anders Dahl, George Vogiatzis, Engin Tola, and Henrik Aanæs. Large scale multi-view stereopsis evaluation. In *Proceedings of the IEEE conference on computer vision and pattern recognition*, pages 406–413, 2014. 6

[19] Mijeong Kim, Seonguk Seo, and Bohyung Han. Infonerf: Ray entropy minimization for few-shot neural volume rendering. In *Proceedings of the IEEE/CVF Conference on Computer Vision and Pattern Recognition*, pages 12912–12921, 2022. 2, 3

[20] Zhengqi Li, Simon Niklaus, Noah Snavely, and Oliver Wang. Neural scene flow fields for space-time view synthesis of dynamic scenes. In *Proceedings of the IEEE/CVF Conference on Computer Vision and Pattern Recognition*, pages 6498–6508, 2021. 2

[21] Chen-Hsuan Lin, Wei-Chiu Ma, Antonio Torralba, and Simon Lucey. Barf: Bundle-adjusting neural radiance fields. In *Proceedings of the IEEE/CVF International Conference on Computer Vision*, pages 5741–5751, 2021. 2

[22] David B Lindell, Julien NP Martel, and Gordon Wetzstein. Autoint: Automatic integration for fast neural volume rendering. In *Proceedings of the IEEE/CVF Conference on Computer Vision and Pattern Recognition*, pages 14556–14565, 2021. 3

[23] Lingjie Liu, Jiatao Gu, Kyaw Zaw Lin, Tat-Seng Chua, and Christian Theobalt. Neural sparse voxel fields. *Advances in Neural Information Processing Systems*, 33:15651–15663, 2020. 1

[24] Quan Meng, Anpei Chen, Haimin Luo, Minye Wu, Hao Su, Lan Xu, Xuming He, and Jingyi Yu. Gnerf: Gan-based neural radiance field without posed camera. In *Proceedings of the IEEE/CVF International Conference on Computer Vision*, pages 6351–6361, 2021. 2

[25] Moritz Menze and Andreas Geiger. Object scene flow for autonomous vehicles. In *Proceedings of the IEEE conference*

*on computer vision and pattern recognition*, pages 3061–3070, 2015. 3

[26] Ben Mildenhall, Pratul P Srinivasan, Rodrigo Ortiz-Cayon, Nima Khademi Kalantari, Ravi Ramamoorthi, Ren Ng, and Abhishek Kar. Local light field fusion: Practical view synthesis with prescriptive sampling guidelines. *ACM Transactions on Graphics (TOG)*, 38(4):1–14, 2019. 5, 6

[27] Ben Mildenhall, Pratul P Srinivasan, Matthew Tancik, Jonathan T Barron, Ravi Ramamoorthi, and Ren Ng. Nerf: Representing scenes as neural radiance fields for view synthesis. In *European conference on computer vision*, pages 405–421. Springer, 2020. 1, 2, 3

[28] Thomas Neff, Pascal Stadlbauer, Mathias Parger, Andreas Kurz, Joerg H Mueller, Chakravarty R Alla Chaitanya, Anton Kaplanyan, and Markus Steinberger. Donerf: Towards real-time rendering of compact neural radiance fields using depth oracle networks. In *Computer Graphics Forum*, volume 40, pages 45–59. Wiley Online Library, 2021. 3

[29] Michael Niemeyer, Jonathan T Barron, Ben Mildenhall, Mehdi SM Sajjadi, Andreas Geiger, and Noha Radwan. Regnerf: Regularizing neural radiance fields for view synthesis from sparse inputs. In *Proceedings of the IEEE/CVF Conference on Computer Vision and Pattern Recognition*, pages 5480–5490, 2022. 1, 2, 3, 6, 7, 12

[30] Albert Pumarola, Enric Corona, Gerard Pons-Moll, and Francesc Moreno-Noguer. D-nerf: Neural radiance fields for dynamic scenes. In *Proceedings of the IEEE/CVF Conference on Computer Vision and Pattern Recognition*, pages 10318–10327, 2021. 2

[31] René Ranftl, Alexey Bochkovskiy, and Vladlen Koltun. Vision transformers for dense prediction. In *Proceedings of the IEEE/CVF International Conference on Computer Vision*, pages 12179–12188, 2021. 2, 4

[32] Christian Reiser, Songyou Peng, Yiyi Liao, and Andreas Geiger. Kilonerf: Speeding up neural radiance fields with thousands of tiny mlps. In *Proceedings of the IEEE/CVF International Conference on Computer Vision*, pages 14335–14345, 2021. 3

[33] Johannes Lutz Schönberger and Jan-Michael Frahm. Structure-from-motion revisited. In *Conference on Computer Vision and Pattern Recognition (CVPR)*, 2016. 2, 3, 16

[34] Nathan Silberman, Derek Hoiem, Pushmeet Kohli, and Rob Fergus. Indoor segmentation and support inference from rgbd images. In *European conference on computer vision*, pages 746–760. Springer, 2012. 3

[35] Vincent Sitzmann, Semon Rezchikov, Bill Freeman, Josh Tenenbaum, and Fredo Durand. Light field networks: Neural scene representations with single-evaluation rendering. *Advances in Neural Information Processing Systems*, 34:19313–19325, 2021. 1

[36] Shuran Song, Fisher Yu, Andy Zeng, Angel X Chang, Manolis Savva, and Thomas Funkhouser. Semantic scene completion from a single depth image. In *Proceedings of the IEEE conference on computer vision and pattern recognition*, pages 1746–1754, 2017. 5

[37] Jürgen Sturm, Nikolas Engelhard, Felix Endres, Wolfram Burgard, and Daniel Cremers. A benchmark for the evaluation of rgb-d slam systems. In *2012 IEEE/RSJ international conference on intelligent robots and systems*, pages 573–580. IEEE, 2012. 3

[38] Towaki Takikawa, Joey Litalien, Kangxue Yin, Karsten Kreis, Charles Loop, Derek Nowrouzezahrai, Alec Jacobson, Morgan McGuire, and Sanja Fidler. Neural geometric level of detail: Real-time rendering with implicit 3d shapes. In *Proceedings of the IEEE/CVF Conference on Computer Vision and Pattern Recognition*, pages 11358–11367, 2021. 3

[39] Matthew Tancik, Vincent Casser, Xinchen Yan, Sabeek Pradhan, Ben Mildenhall, Pratul P Srinivasan, Jonathan T Barron, and Henrik Kretzschmar. Block-nerf: Scalable large scene neural view synthesis. In *Proceedings of the IEEE/CVF Conference on Computer Vision and Pattern Recognition*, pages 8248–8258, 2022. 2

[40] Haithem Turki, Deva Ramanan, and Mahadev Satyanarayanan. Mega-nerf: Scalable construction of large-scale nerfs for virtual fly-throughs. In *Proceedings of the IEEE/CVF Conference on Computer Vision and Pattern Recognition*, pages 12922–12931, 2022. 2

[41] Zhou Wang, Alan C Bovik, Hamid R Sheikh, and Eero P Simoncelli. Image quality assessment: from error visibility to structural similarity. *IEEE transactions on image processing*, 13(4):600–612, 2004. 6

[42] Zirui Wang, Shangzhe Wu, Weidi Xie, Min Chen, and Victor Adrian Prisacariu. Nerf–: Neural radiance fields without known camera parameters. *arXiv preprint arXiv:2102.07064*, 2021. 2

[43] Suttisak Wizadwongsa, Pakkapon Phongthawee, Jiraphon Yenphraphai, and Supasorn Suwajanakorn. Nex: Real-time view synthesis with neural basis expansion. In *Proceedings of the IEEE/CVF Conference on Computer Vision and Pattern Recognition*, pages 8534–8543, 2021. 3

[44] Wenqi Xian, Jia-Bin Huang, Johannes Kopf, and Changil Kim. Space-time neural irradiance fields for free-viewpoint video. In *Proceedings of the IEEE/CVF Conference on Computer Vision and Pattern Recognition*, pages 9421–9431, 2021. 2

[45] Yuanbo Xiangli, Linning Xu, Xingang Pan, Nanxuan Zhao, Anyi Rao, Christian Theobalt, Bo Dai, and Dahua Lin. Citynerf: Building nerf at city scale. *arXiv preprint arXiv:2112.05504*, 2021. 2

[46] Dejia Xu, Yifan Jiang, Peihao Wang, Zhiwen Fan, Humphrey Shi, and Zhangyang Wang. Sinnerf: Training neural radiance fields on complex scenes from a single image. *arXiv preprint arXiv:2204.00928*, 2022. 3

[47] Alex Yu, Ruilong Li, Matthew Tancik, Hao Li, Ren Ng, and Angjoo Kanazawa. Plenoctrees for real-time rendering of neural radiance fields. In *Proceedings of the IEEE/CVF International Conference on Computer Vision*, pages 5752–5761, 2021. 3

[48] Alex Yu, Vickie Ye, Matthew Tancik, and Angjoo Kanazawa. pixelnerf: Neural radiance fields from one or few images. In *Proceedings of the IEEE/CVF Conference on Computer Vision and Pattern Recognition*, pages 4578–4587, 2021. 2, 3, 6, 7

[49] Zehao Yu, Songyou Peng, Michael Niemeyer, Torsten Sattler, and Andreas Geiger. Monosdf: Exploring monocu-

lar geometric cues for neural implicit surface reconstruction. *arXiv preprint arXiv:2206.00665*, 2022. 1, 2, 3, 4, 7, 8

[50] Richard Zhang, Phillip Isola, Alexei A Efros, Eli Shechtman, and Oliver Wang. The unreasonable effectiveness of deep features as a perceptual metric. In *Proceedings of the IEEE conference on computer vision and pattern recognition*, pages 586–595, 2018. 6

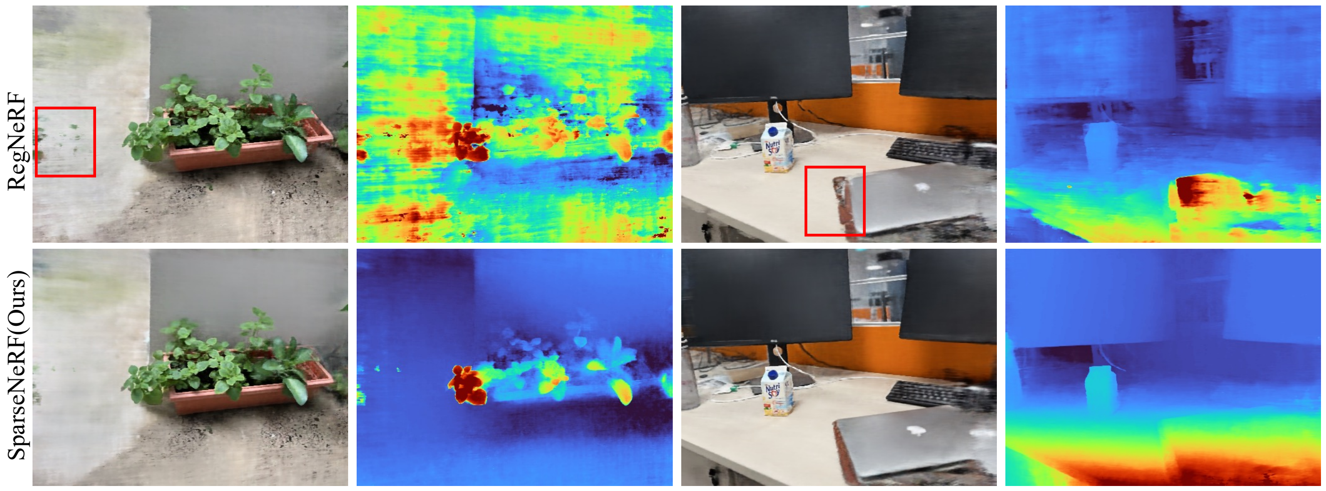

Figure 9: Applications on iPhone 13 Pro. We use three RGDB images for training. Depth maps are captured by iPhone's LiDAR. Comparing the state-of-the-art RegNeRF [29] and the proposed SparseNeRF with three views for training, our method can extract useful depth priors from the model and synthesize realistic novel views and coherent geometric depth even though only three training views are available (Please refer to the demo videos for rendered videos).

## A. Applications

### A1. Few-shot NeRF on iPhone

Apple's latest products (iPhone 12 Pro and higher versions, and iPad Pro now feature built-in LiDAR sensors that can capture depth maps. We use the portrait mode of iPhone 13 Pro to collect RGBD datasets. We train RegNeRF and SparseNeRF with three views (RGB images and depth maps are aligned), and rendered novel views, as shown in **Figure 9**. RegNeRF does not recover a correct geometry while the proposed SparseNeRF significantly improves the reconstruction of geometry. The main reason is that RegNeRF adds a geometric continuity constraint from unseen viewpoints such that neighbor depth pixels should be as close as possible. This regularization does not fully exploit the depth priors of objects/scenes. Instead, the proposed SparseNeRF distills the depth ranking and the spatial continuity of depth maps captured by an iPhone's LiDAR, which achieves promising rendered results.

### A2. Few-shot NeRF with Simple User-click Depth Annotations

The SparseNeRF significantly improves few-shot novel view synthesis with the help of coarse depth maps, obtained by pre-trained depth models and consumer-level sensors. What if the depth rankings of partial regions of depth maps are incorrect in some cases? Do we have any ideas to fix this issue? We give an application that fixes incorrect depth rankings of pre-trained depth or sensors when we do not trust these coarse depth maps. As shown in **Figure 10** **(a)**, users can easily click near-far depth pairs in a local region, e.g., depth pairs in cyan circles. Green points are nearer while red points are farther. In **Figure 10** **(b)** and **Figure 10** **(c)**, we train a few-shot NeRF without and with user-click depth annotations, respectively. It is observed that the performance of the few-shot NeRF significantly improves. In practice, 30$\sim$40 depth pairs of each view lead to significant improvement. In real-world scenes, one may only need to annotate partial regions for refinement. User-click depth annotations provide sparse depth rankings, which tailors for the proposed SparseNeRF. In real-world applications, occlusion often occurs in complex scenes. Even with dense views for training, some regions are observed from a limited number of views. Therefore, this application helps dense-view NeRF to refine novel view synthesis in these cases.

## B. Detailed Descriptions of the new Dataset NVS-RGBD

In **Section 4**, we give a brief introduction to our new dataset NVS-RGBD. In this material, we provide a detailed description. Different from previous methods that derive accurate and expensive ground-truth depth maps by pre-trained NeRF trained with dense views [12] or captured by high-accuracy depth scanners [11], our goal is to develop a good NeRF with cheap or even free coarse depth maps, i.e., pre-trained single-view depth estimation models and consumer-level depth sensors. To this end, we use Microsoft Azure Kinect, ZED 2, and iPhone 13 Pro to collect a new dataset NVS-RGBD. For each sensor, we collect 8 scenes, which is similar to the LLFF dataset that focuses on forward-facing scenes. For each scene, we evenly sample 3 views for training and the held-out views are for testing.

The examples of the NVS-RGBD dataset are shown in **Figure 11**. As for Azure Kinect, the edges of objects often contain lots of noise. Some regions are directly masked by

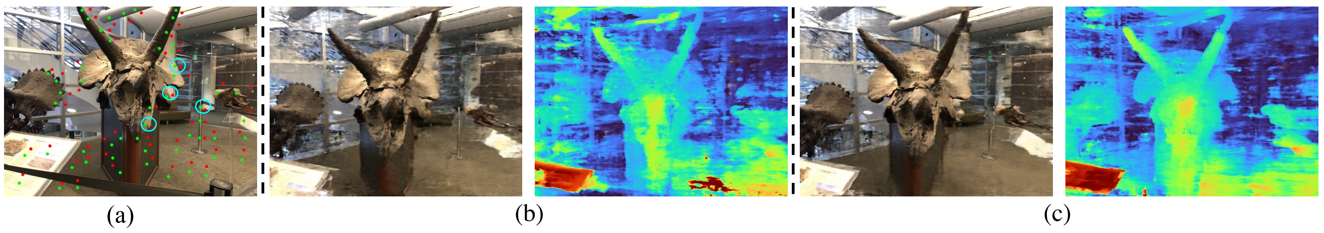

Figure 10: Application with simple user-click depth annotations. Annotators are required to click near-far depth pairs in a local region (e.g., near-far pairs in cyan circles). Green points are nearer while red points are farther. (a) User-click depth annotations. (b) Without user-click depth annotations. (c) With user-click depth annotations. User-click depth annotations provide sparse depth rankings, which tailors for the proposed SparseNeRF.

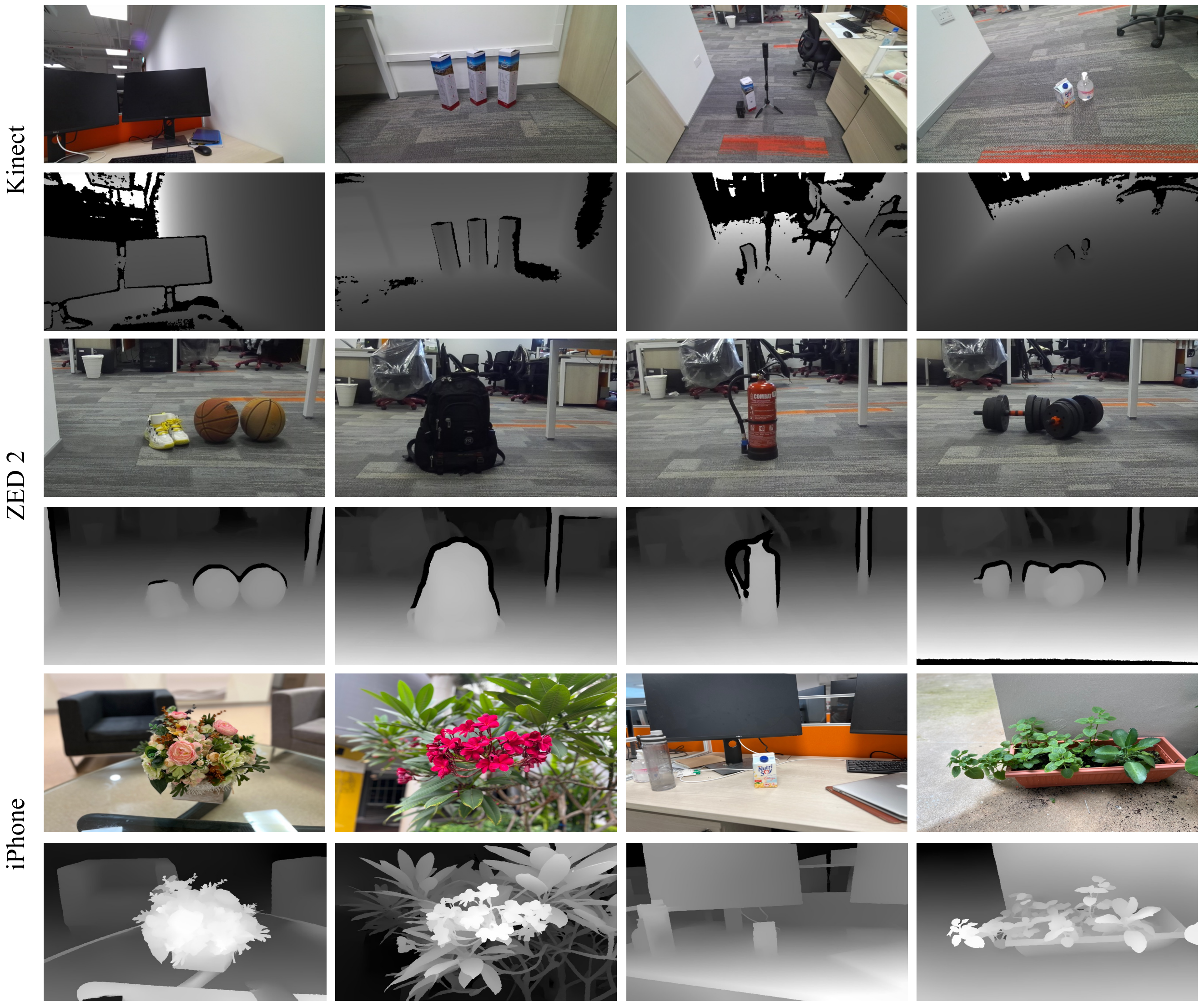

Figure 11: Examples of the NVS-RGBD dataset. It contains RGBD images captured by Azure Kinect, ZED 2, and iPhone.

sensors. As for ZED 2, the edges of the depth maps are inaccurate. In **Figure 3**, we observe that the depth maps of ZED 2 look smooth but unstable and incorrect when observing time jittering. We masked out the uncertain black regions of

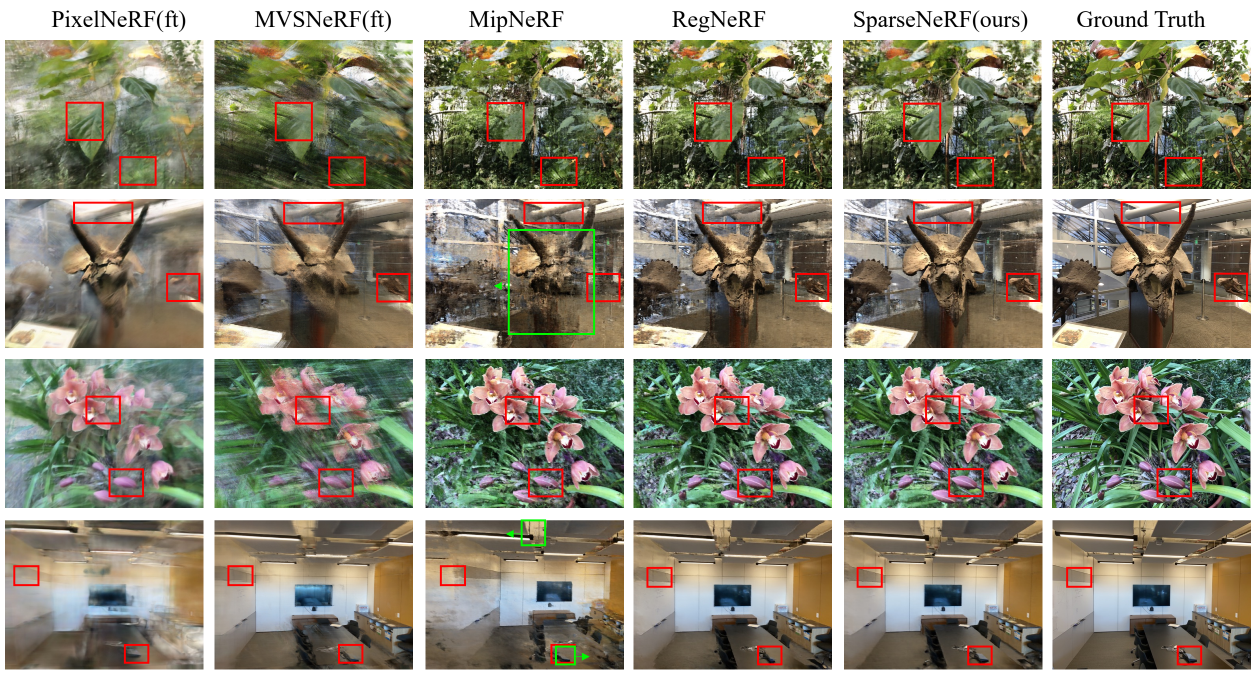

Figure 12: Visual comparisons on the LLFF dataset with three views. Red boxes denote compared regions. Green boxes denote shifted objects. SparseNeRF achieves consistent improvement in different scenes.

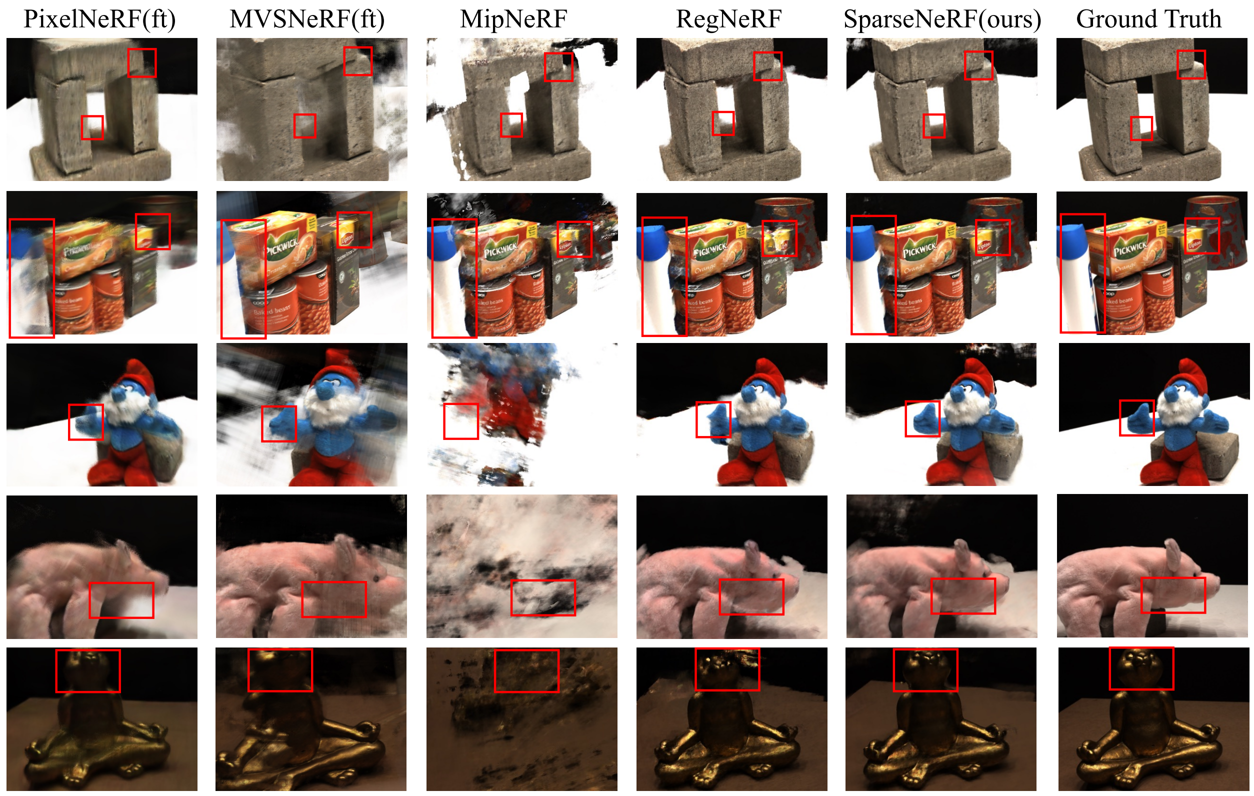

Figure 13: Visual comparisons on the DTU dataset with three views. Red boxes denote compared regions. SparseNeRF achieves consistent improvement in different scenes.

depth maps for training. Moreover, the scale of these depth maps is not linearly scaled to the ground-truth depth maps

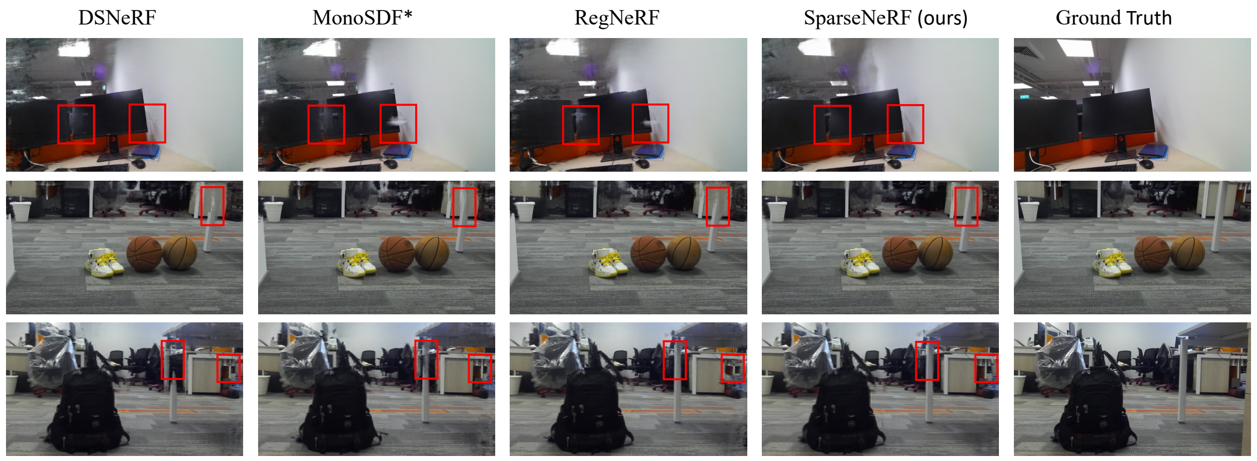

Figure 14: Visual comparisons on the NVS-RGBD dataset with three views. Red boxes denote compared regions. SparseNeRF achieves consistent improvement in different scenes.

predicted by dense-view NeRFs. As for the depth maps of the iPhone, they are more smooth than Kinect and ZED 2. The drawback is that the distance between objects and the iPhone is up to 2.5 meters.

## C. More Implementation Details

We implement SparseNeRF based on the official JAX [3]. We use the Adam optimizer for the learning of SparseNeRF. We use an exponential learning rate, which decays from $2 \times 10^{-3}$ to $2 \times 10^{-5}$. The batch size is set to 4096. For each scene, we use one GPU-v100 with 32G memory for both training and inference. We also implement the proposed SparseNeRF on GPU-v100 with 16G and RTX 2080 Ti with 11G. We reduce the batch size to 2048 and 1024 for these two types of GPUs, respectively. We use the same backbone and sampled points along rays compared with prior arts.

We train 60k iterations for each scene given three training views, which takes about 1.5 hours for each scene. For depth maps captured by Kinect and ZED 2, we mask uncertain regions (black regions in depth maps). More precisely, we sample near-far depth pairs in certain regions in local patches to optimize **Eqs.** 3 and 4 of the paper.

In **Tables** 1 and 2 of the paper, 5 and 6, we reproduce most of the prior arts as the supplementary Material of RegNeRF. we implement DSNeRF as the official codebase. In **Table** 7, MonoSDF is mainly designed for surface reconstruction. We apply the depth consistency loss to RegNeRF for novel view synthesis of RGB images for comparison. The depth consistency loss is a scale-invariant loss constrained in local patches. In **Table** 3, we can see that MonoSDF obtains a lower depth error than RegNeRF, but fails to achieve better novel view synthesis of RGB images.

## D. More Visual Comparisons

In **Figures** 5, 6, and 7 of the main body of the paper, we give two examples of visual comparisons. In this material, **Figures** 12, 13, and 14 show more visual examples on the LLFF, DTU, and NVS-RGBD datasets, respectively. In particular, we compare five representative methods on LLFF and DTU, respectively. Among them, MipNeRF is a state-of-the-art NeRF method designed for conventional dense-view NeRF, which is optimized by color reconstruction. Without extra geometric regularization, MipNeRF fails to synthesize good novel views. As shown in **Figures** 12 and 13, it is observed that positions of objects predicted by MipNeRF might be shifted due to the underconstrained problem. PixelNeRF(ft) and MVSNeRF(ft) require pre-training on extra scenes and fine-tuning on a target scene. Thanks to the pre-training, PixelNeRF(ft) and MVSNeRF(ft) greatly improve few-shot NeRFs. Compared with PixelNeRF(ft) and MVSNeRF(ft), RegNeRF and SparseNeRF do not require extra scenes for pre-training. RegNeRF optimizes few-shot NeRF by adding a continuous geometric constraint from unseen viewpoints such that the depth values of neighbor pixels should be as close as possible. RegNeRF achieves a new state-of-the-art performance but fails to guarantee the correct geometry of objects. Unlike RegNeRF, the proposed SparseNeRF exploits coarse depth maps of pre-trained depth models in the experiments. Thanks to the distillation of depth ranking and spatial continuity of petrained depth models, SparseNeRF significantly improves few-shot NeRFs.

In **Figures** 12 and 13, SparseNeRF distills depth priors from pre-trained depth models. In **Figure** 14, we use depth sensors to collect coarse depth maps. We compare two depth-based methods and the best few-shot NeRF method RegNeRF. Among them, DSNeRF adopts sparse

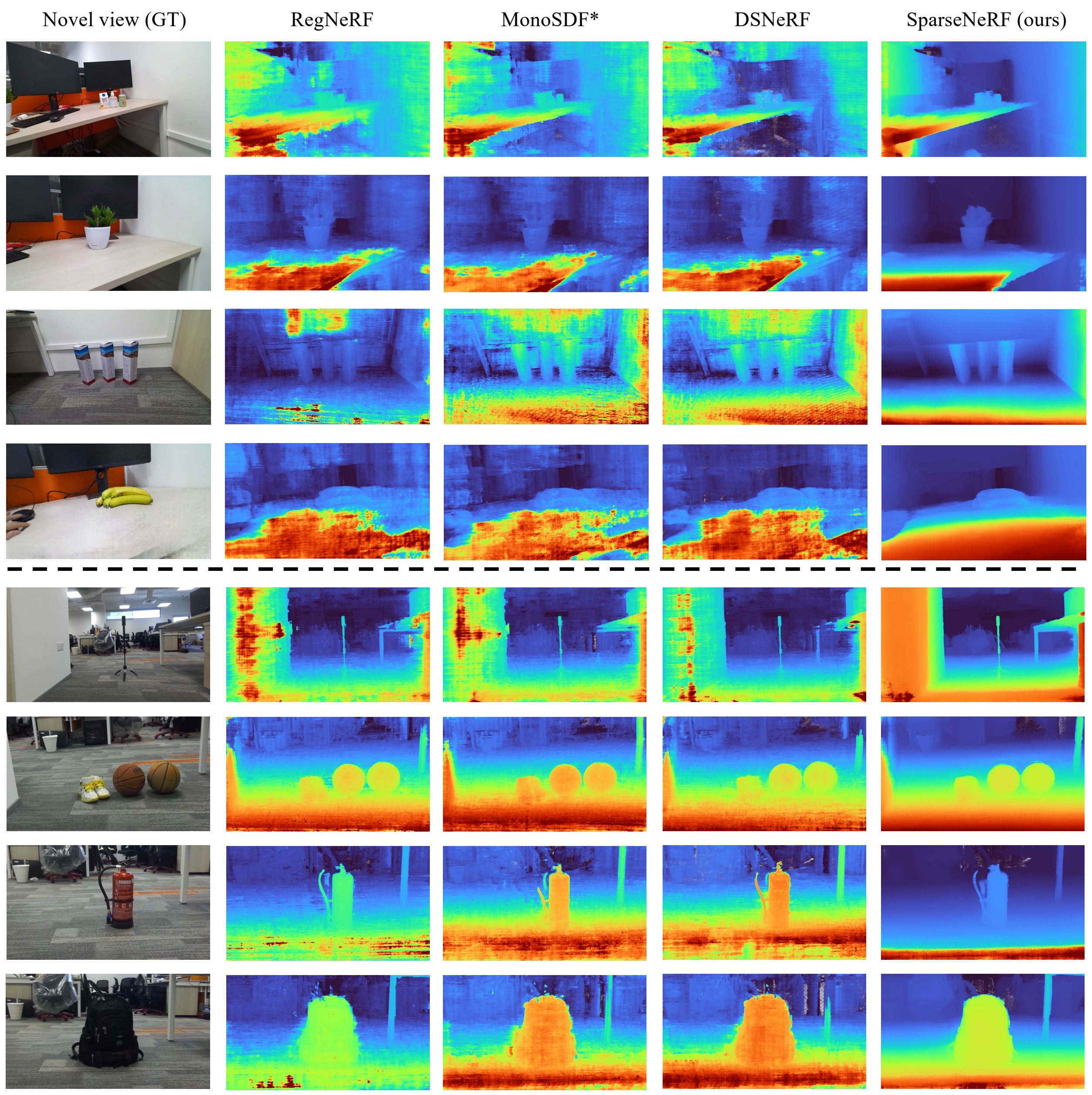

Figure 15: Visual comparisons of predicted geometry. Top: captured by Azure Kinect. Bottom: captured by ZED 2.

3D points derived by the COLMAP algorithm [33]. We implement depth-supervised loss of DSNeRF upon RegNeRF. MonoSDF is originally proposed for surface reconstruction. We implement the depth consistency loss upon RegNeRF, which encourages the predicted depth to be scale-invariant to coarse depth maps. The drawback of this method is the strong assumption about the scale-invariant depth constraint. The cheap depth maps from pre-trained single-view depth models or consumer-level depth sensors are incorrect. They only provide coarse geometry information. We will study the depth errors in **Section F**. Compared with the two depth-based NeRFs and the best few-shot NeRF RegNeRF, the proposed SparseNeRF achieves a better visual effect.

## E. Visual Comparisons of Predicted Geometry

In **Table 3** of the paper, we compare the scale-invariant depth errors of four few-shot NeRF methods. The results show that the SparseNeRF significantly outperforms RegNeRF, i.e., from $5.9\times10^{-3}$ to $3.9\times10^{-3}$ on the scenes captured by Kinect and from $3.5\times10^{-3}$ to $2.4\times10^{-3}$ on the scenes captured by ZED 2. DSNeRF and MonoSDF also improve RegNeRF on depth errors. The depth error indicates the quality of the reconstructed geometry.

In this material, we study the qualitative results of geometry, as shown in Figure 15. The top four rows show the comparisons on the RGBD data of Kinect. The bottom four rows are for ZED 2. Compared with RegNeRF, DSNeRF uses sparse 3D points for depth supervision. MonoSDF imposes a local scale-invariant loss computed by coarse depth maps and predicted depth of NeRFs. Compared with RegNeRF, MonoSDF, and DSNeRF, SparseNeRF yields much better geometry. The sub-optimal results of MonoSDF can be attributed to the fact that coarse depth maps are not able to be linearly scaled to ground-truth depth maps. In the next section, we will analyze the scale-invariant depth errors of coarse depth maps.